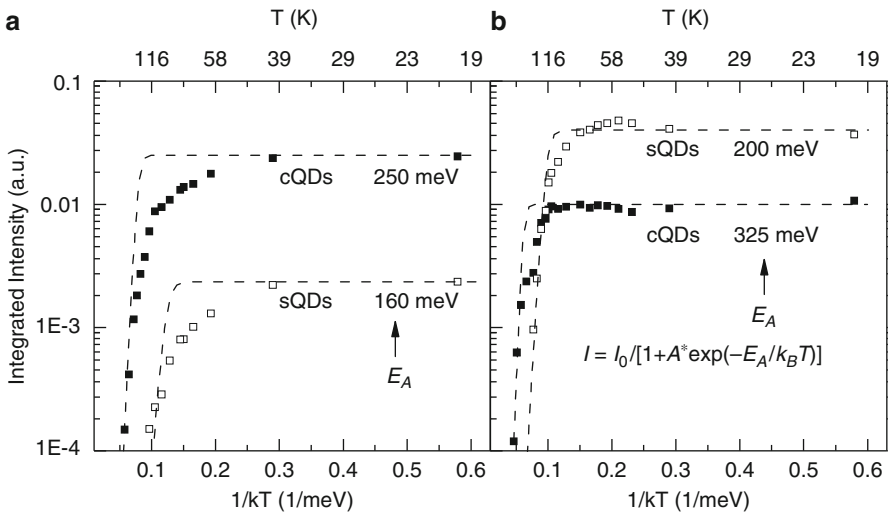

Fig. 3.8 Integrated intensities of cQDs- and sQDs-related spectra for (**a**) 1.8/25/1.2 and (**b**) 1.8/25/1.5 QDMs, plotted as a function of temperature T and $1/k_BT$. The *filled-square* and *open-square* symbols are measured values for cQDs- and sQDs-related spectra, respectively. The *dashed lines* are single activation energy fittings with pre-exponential factor $A = 3 \times 10^8$ and E_A as indicated. Reproduced from [35] with permission from Elsevier

cQDs and 160 meV for sQDs, and in the 1.8/25/1.5 QDMs are 325 meV for cQDs and 200 meV for sQDs. These values agree with the energetic difference between the related peak energy and the WL energy. The fits for the 1.8/25/1.5 QDMs are excellent: the cQD peak at 1.075 eV and the sQD peak at 1.195 eV are lower than the 1.4-eV WL energy by 325 and 205 meV, respectively. The matches are almost exact. The fits for the 1.8/25/1.2 QDMs are satisfactory for sQDs only: the cQD peak at 1.075 eV and the sQD peak at 1.240 eV are lower than the 1.4-eV WL energy by 325 and 160 meV, respectively. The corresponding best fits values are 250 and 150 meV. It is unclear what causes the large discrepancy in the case of cQDs but possible causes include the presence of some small percentage of excited-state excitons (which lowers the effective potential barrier or activation energy) or defects in or around the nanohole-and-mound template (which introduces NRR centers/channels).

3.5 Stacked QDMs

The existence of two ground-state energies makes lateral QDMs a promising candidate as a broadband material for near-infrared (NIR) emissions, especially if more than one active layer is present. It is typical for quantum wells (QWs) or QDs active layers employed in superluminescent diodes (SLDs) to be chirped,

i.e. stacked in the growth direction where each layer is grown differently [46, 47]. Broadband SLDs find applications in various fields, the most prominent of which is possibly as the broadband source at the heart of optical coherence tomography (OCT) [48]. The resolution of images acquired from OCT is inversely proportional to the luminescent linewidth (FWHM) of the NIR source [49]. We proposed and demonstrated that lateral QDMs are well suited as an active material for broadband devices and systems. The main advantage over conventional QDs or QWs-based chirped structures is the broader FWHM for the same number of stacked layer, or smaller number of stacked layers for the same FWHM. This section describes chirping schemes based on lateral QDMs bi-layers as the active material. The bi-layers comprise four nominally different sub-ensembles; the PL in each of which has a predictable temperature dependency, allowing easy design and optimization of structures with a greater number of stacks.

3.5.1 Chirped Bi-Layers

A single layer of lateral QDMs exhibits two GS energies: a low-energy, narrow emission from cQDs and a high-energy, broad emission from sQDs. A lateral QDMs bi-layer thus exhibits four GS energies which, in order to maximize the FWHM for broadband applications, can be designed to overlap in accordance with one of the three schemes shown in Fig. 3.9a–c [23].

The straddled scheme or Type-I chirp depicted in Fig. 3.9a makes use of a wide separation between the two GS energies of one layer (cQD_1 and sQD_1 in the figure, unshaded curves) to straddle or sandwich the narrow separation of the other (cQD_2 and sQD_2, shaded). The wide separation can be achieved by a relatively thick capping and regrowth, a condition where cQDs are filled but sQDs are forming and still far from saturation. The 1.8/25/1.5 QDMs described in Sect. 3.4.2, for example, meet this criteria. The spectrum shown in Fig. 3.5b indicates GS separation as wide as 145 meV. The narrow separation, on the other hand, can be achieved by a relatively thin capping and thick regrowth. The 2/6/1.4 QDMs described in Sect. 3.4.1 with PL spectrum in Fig. 3.4b, for example, show the separation of almost zero as the cQD and sQD GS peaks are unresolved. Alternatively, a single cQD peak can be employed. By growing a bi-layer of 2/26/2 QDM_1 and 2/26/1.4 QDM_2, a Type-I chirp spectrum can be obtained. (Subscripts 1 and 2 indicate, respectively, the lower and upper QDM layers in the growth sequence.) Figure 3.9d shows the PL spectra of the bi-layer (upper spectrum) with respect to the controlled, single layer 2/25/1.4 QDMs. The latter, previously shown as a linear plot in Fig. 3.4b, exhibits a single PL peak since the deep nanoholes have yet to be saturated. The former exhibits three GS peaks: the minimum at 1.048 eV and the maximum at 1.214 eV are from the 2/26/2 QDM_1, whereas the intermediate peak at 1.086 eV is from the 2/26/1.4 QDM_2. Multi-Gaussian function fits (dashed lines) show that the lower two peak energies are narrow, indicative of cQDs-based origin, and the high peak energy is broad, indicative of sQDs-based origin. The intermediate peak energy from the

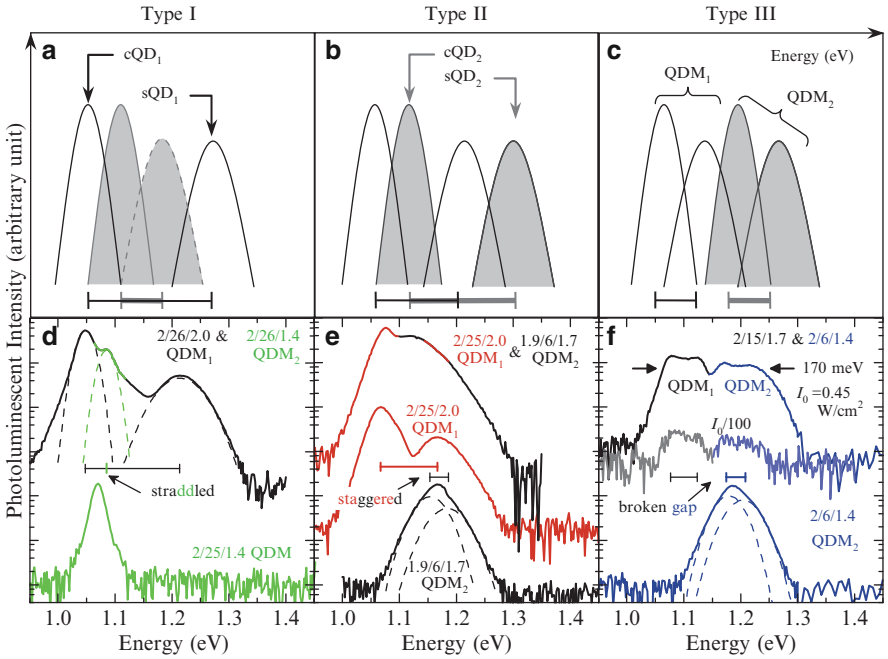

Fig. 3.9 Schematic spectral superposition of (**a**) straddled or Type-I, (**b**) staggered or Type-II, and (**c**) broken-gap or Type-III chirped QDM bi-layers. The *black* (*gray*) *bar* marks the spectral range between the cQD and sQD peaks of QDM_1 (QDM_2). Subscripts 1 and 2 denote the lower and upper QDM layers, respectively. Measured 20 K PL spectra of samples containing single QDM layer or chirped QDM bi-layer as active layers: (**d**) single 2/25/1.4 QDMs reference (*lower plot*), and chirped 2/26/2.0 QDM_1 bottom layer and 2/26/1.4 QDM_2 top layer (*upper*); (**e**) single 1.9/6/1.7 QDM_2 (*lower*), single 2/25/2.0 QDM_1 (*middle*), and chirped QDM_1/QDM_2 bi-layer (*upper*); and (**f**) single 2/6/1.4 QDM_2 (*lower*), and chirped 2/15/1.7 QDM_1 and 2/6/1.4 QDM_2 bi-layer under nominal (*upper*) and reduced excitations (*middle*). *Dashed lines* in (**d**–**f**) are multiple Gaussian function fits. Spectra are offset for clarity. Adapted from [23]

2/26/1.4 QDM_2 is sandwiched between the minimum and maximum from the 2/26/2 QDM_1 as expected and provides a smoothening effect of the whole spectrum. The bi-layer spectrum clearly demonstrates the superposition of individual PL peaks, indicating that reabsorptions are insignificant.

The staggered scheme or Type-II chirp depicted in Fig. 3.9b makes use of two QDM ensembles with similarly wide energetic separations and which are offset along the energy scale. One possible implementation as shown in Fig. 3.9b positions cQD_2 between cQD_1 and sQD_1, and sQD_1 between cQD_2 and sQD_2. This can be achieved by designing the bi-layers to have different capping thickness, to ensure separated cQD peak energies, but similar regrowth thickness. Figure 3.9e shows the PL spectra of the 2/25/2 QDM_1 and 1.9/6/1.7 QDM_2 bi-layer (upper spectrum) with respect to the controlled, single layers of 2/25/2 QDM_1 (middle) and 1.9/6/1.7 QDM_2 (lower). The lower spectrum shows the almost merged cQDs and sQDs

peaks, similar to the 2/6/1.4 QDMs spectrum in Fig. 3.4b. The Gaussian fits (dashed lines in the lower spectrum) reveal the constituent cQDs and sQDs peaks. The middle spectrum shows two well-separated cQD and sQD peaks. The four peaks from the lower and middle spectra are staggered in accordance with the design in Fig. 3.9b. The dip in the middle of QDM_1's spectrum is made up by the rapid rise at the same energetic position of QDM_2's spectrum, resulting in a smoothened overall spectrum in the QDMs bi-layer. The bi-layer spectrum demonstrates that with proper design a broad Gaussian spectrum can be obtained.

The broken-gap scheme or Type-III chirp depicted in Fig. 3.9c makes use of two QDM ensembles with similarly narrow energetic separations where the highest peak energy of one QDM ensemble is lower than the lowest peak energy of the other. This can be achieved by designing the bi-layers to have different capping thickness, to ensure separated cQD peak energies as in Type II, and similarly thick regrowth, to ensure narrow cQD–sQD separation. Figure 3.9f shows the PL spectra of the 2/15/1.7 QDM_1 and 2/6/1.4 QDM_2 bi-layer (upper spectrum) with respect to the controlled, single layer of 2/6/1.4 QDM_2 (lower). The existent of multiple peaks in the upper spectrum of the bi-layers begs the question as to whether all these four peaks are GS. To answer this we reduce the excitation power density by two orders of magnitude, observe the linear decrease of the four peaks down to almost the noise floor as shown in the middle spectrum, and thus confirm that all the peaks in the upper spectrum are indeed GS peaks. Ignoring the small dip in the middle, the spectrum has a broad FWHM of 170 meV. This non-optimized value by chirping *two* layers of lateral QDMs compares favorably with 125 meV obtained from chirping *four* layers of QDs [47], or 200 meV from *sixty* stacks of strain-compensated structure [50]. Lateral QDM bi-layers thus provide the best active layer in terms of cost-performance: a broader FWHM can be achieved for the same stack number, or the smallest stack number is required for the same FWHM.

3.5.2 Temperature Dependencies

The optical properties of a lateral QDM *single* layer has been shown to follow the bimodal optical characteristics explained in Sect. 3.4.3, it is thus expected that the *bi*-layer should follow the same temperature dependencies since both layers are separated by a thick 100-nm GaAs spacer layer and hence should be optically uncoupled. Though reabsorptions (of QDM_1 emissions by QDM_2, and vice versa) are a concern, low-temperature PL spectra in the three chirping schemes above indicate that they do not qualitatively affect the wavelength superposition. Variable temperature PL spectra in this section additionally indicate that they do not qualitatively affect the underlying carrier escape and redistribution from and between cQDs and sQDs either.

The temperature-dependent PL spectra of the Types I–III chirped samples above are shown in Fig. 3.10a–c, respectively. The overall spectra are similarly quenched as the temperature increases, and beyond 250 K no luminescence can be measured.

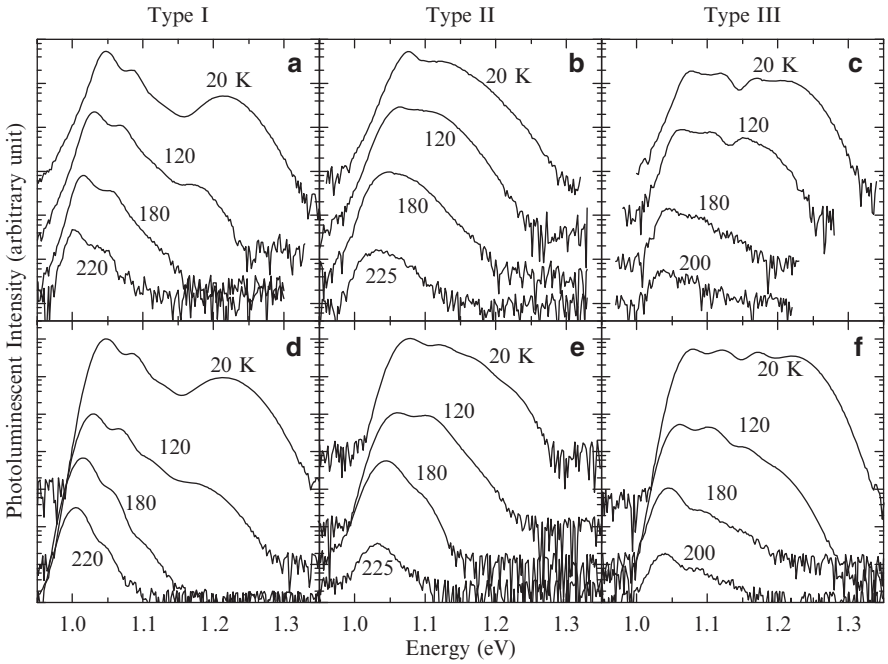

Fig. 3.10 Temperature-dependent PL of chirped QDM bi-layers: measured PL spectra of Types (**a**) I, (**b**) II, and (**c**) III; simulated PL spectra of Types (**d**) I, (**e**) II, and (**f**) III. Line spectra in (**a**–**f**) are offset for clarity. Simulated line spectra in (**d**–**f**) are performed at the same temperatures as the measured spectra in (**a**–**c**), respectively. Adapted from [23]

This is not to be taken as a limiting factor for room-temperature operations as the structures have yet to be optimized. The overarching trend in all samples is the subsequent quenching from the high-energy ends. In Fig. 3.10a, for example, the highest-energy peak at 1.214 eV is the first to be quenched, followed by the next immediate peak at 1.086 eV, and finally by the lowest-energy peak at 1.048 eV. Such orderly quenching is characteristic of thermal activation of carriers out of QDs into the adjacent WL and/or GaAs matrix where carriers recombine non-radiatively. The multiplicity of luminescent peaks in the QDM bi-layers makes it difficult to identify the NRR channels and associated activation energies without prior knowledge from controlled single QDM layer structures. If our hypothesis of optical independence between the QDM bi-layer is correct, the main escape channel should be the same as QDM single layers, i.e. the WL as identified by the Arrhenius plots in Fig. 3.8.

In order to identify the NRR channels and to understand the temperature dependencies of the three chirp structures, the spectra are fitted to the equation:

$$I = \sum_{i=1}^{4} \frac{I_i \exp{(E - E_i)^2}/\Gamma_i^2}{1 + A \exp{-(E - E_{\mathrm{WL}})}/\eta_i k_{\mathrm{B}} T}$$

Table 3.1 Simulation parameters for the PL maps and spectra of chirped QDM bi-layers

	QDM_1		QDM_2	
	cQD_1	sQD_1	cQD_2	sQD_2
Type I—straddled				
I_i	1.000	0.094	0.358	0.071
E_i (eV)	1.048	1.214*	1.085	1.114*
FWHM (meV)	30.6	77.7*	28.3	51.8*
η_i	1.0–1.6	1.1–1.9	1.0–1.6	1.1–1.9
Type II—staggered				
I_i	1.000	0.315	0.591	0.044
E_i (eV)	1.077	1.160*	1.120	1.213*
FWHM (meV)	40.0	53.0*	40.0	49.5*
η_i	1–1.4	1–1.8	1–1.4	1–1.8
Type III—broken-gap				
I_i	1.0	1.0	0.7	0.7
E_i (eV)	1.078	1.121	1.170	1.220*
FWHM (meV)	33.0	42.4	33.0	65.9*
η_i	1.1–2	1.1–2	1.1–2	1.0–2

Twenty-Kelvin peak energy position E_i, relative intensity I_i, and FWHM of cQDs and sQDs ensembles of Types I–III chirped QDM bi-layers extracted from Fig. 3.10a–c, respectively. The ideality factor η_i varies linearly with temperature from the lower limit value at 20 K to the upper limit value at 300 K. Subscripts 1 and 2 represent the lower and upper QDM layers, respectively. E_i's temperature dependency follows Varshni's equation unless marked by * where it instead follows the sigmoidal behavior. FWHM is assumed constant unless marked by * where it follows the anomalous temperature behavior. The FWHM is related to the standard deviation of the Gaussian distribution or the broadening parameter Γ through the relationship: FWHM (meV) $= 1{,}665.11 \times \Gamma$. Reproduced from [23]

where the overall intensity I at energy E and temperature T is a summation of constituent intensities from QDM_1 (cQD_1 and sQD_1) and QDM_2 (cQD_2 and sQD_2), hence the summation from $i = 1$ to 4. Each constituent's luminescence has a low-temperature intensity I_i at a peak energy E_i, a broadening parameter Γ_i and is quenched by thermal escape to the WL level E_{WL}. A is the pre-exponential factor, k_B is the Boltzmann's constant and η_i is the ideality factor indicating the dominance of the WL over other NRR channel(s). If the WL is the sole factor responsible for quenching, then $\eta_i = 1$. If other NRR channel(s) co-exist and acting in parallel, then $\eta_i > 1$. The further η_i is from 1, the less significant the WL is as excitons escape route. The fitting parameters extracted from the measured spectra are summarized in Table 3.1.

The simulated line spectra of Types I–III chirps at selected temperatures are shown underneath the measured spectra in Fig. 3.10d–f, respectively. A white noise is added to the simulated data to reflect the actual noise levels in our setup. The full simulations of Types I–III chirps covering the 20–300 K temperature range are shown in the PL maps $I(E, T)$ in Fig. 3.11a–c, respectively. The dashed lines

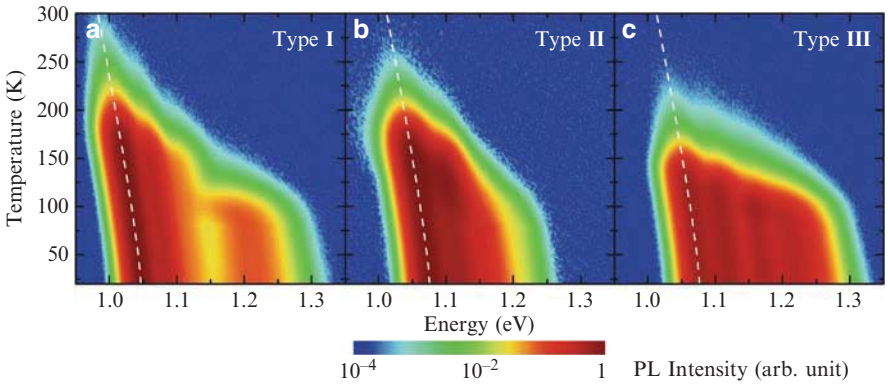

Fig. 3.11 Simulated PL maps $I(E, T)$ of Types (**a**) I, (**b**) II, and (**c**) III chirped QDM bi-layers. *Dashed lines* are bandgap variations with temperature according to Varshni's equation with bulk InAs parameters, linearly shifted to match the lowest-energy cQD peaks. Adapted from [23]

in the PL maps are calculated temperature variations of the cQD peak based on Varshni's equation and bulk InAs parameters; the trend is followed only by cQDs-related peaks. Despite the simplicity of the approach, the fits predict all the major characteristics of the measured spectra at all experimental temperatures. Though we can further improve the simulations by incorporating the recently reported parameters for the Fan model [37], it does not change the qualitative nature of our conclusions that the WL is the main escape path and that the activation energy falls somewhere between the ideal case where $\eta_i = 1$ and the limiting case where $\eta_i = 2$.

Though the chirping schemes described in Sect. 3.5.1 and the demonstrated optical characteristics in Sect. 3.5.2 employ a QDM bi-layer as the active layer, the same fundamental concepts can be readily extended to structures with number of stacks greater than two, or to other material systems in order to increase the bandwidth or to shift the nominal wavelength to other region of the electromagnetic spectrum, respectively.

3.6 Conclusion

Lateral InGaAs quantum dot molecules are grown by solid-source MBE via the partial-cap and regrowth process using the nanohole-and-mound template. Each QDM comprises two types of QDs: a cQD located at the nanohole center, and sQDs surrounding it. Differences in nucleation locations and dynamics result in cQDs and sQDs having different sizes and degrees of homogeneity: cQDs are generally taller and more uniform than sQDs. Temperature-dependent photoluminescent spectra reflect the geometrical differences: cQDs typically emit at a low GS energy around 1.05 eV with a narrow FWHM below 30 meV whereas sQDs emit at about 150 meV higher with a broad FWHM that more than doubles

those of cQDs. As sample temperature varies, cQDs emission is found to simply follow the InAs bulk bandgap variation in accordance with Varshni's equation. On the contrary, sQDs exhibit a sigmoidal temperature behavior resulting from carrier redistribution among inhomogeneous QDs. The two qualitatively different temperature-dependent PL or the bimodal *optical* property results from the intrinsic bimodal *size* distribution of our lateral QDM ensemble. With this unique property we proposed and demonstrated a QDM bi-layer structure that exhibits four GS energies whose spectra can be arranged to overlap in three basic configurations: straddled, staggered, and broken-gap. A non-optimized, proof-of-principle structure shows a broadband spectrum with FWHM of 170 meV. The spectra are well explained by multi-Gaussian functions with carrier redistributions among sQDs and quenching via thermal escape and recombination via the wetting layer and non-radiative recombination centers/channels acting in parallel. We introduced an ideality factor to indicate the dominance of the WL as the quenching channel. Well-understood optical properties of lateral QDM single- and bi-layers are necessary if they are to serve as an active material for devices destined for broadband absorption such as solar cells or for broadband emissions such as superluminescent diodes.

Acknowledgments AFM data analyses are performed using Gwyddion. This work is supported by Thailand Research Fund (RSA5580015, DPG5380002); Nanotec; Integrated Innovation Academic Center (IIAC), Chulalongkorn University Centenary Academic Development Project; and the Higher Education Research Promotion and National Research University Project of Thailand, Office of the Higher Education Commission (CU56-EN09).

References

1. Leonard, D., Krishnamurthy, M., Reaves, C.M., Denbaars, S.P., Petroff, P.M.: Appl. Phys. Lett. **63**, 3203 (1993)
2. Bimberg, D., Grundmann, M., Ledentsov, N.N.: Quantum Dot Heterostructures. Wiley, Chichester (1999)
3. Wang, Z.M. (ed.): Self-Assembled Quantum Dots. Lecture Notes in Nanoscale Science and Technology. Springer, New York (2007)
4. Watanabe, K., Koguchi, N., Gotoh, Y.: Jpn. J. Appl. Phys. **39**, L79 (2000)
5. Wang, L., et al.: New J. Phys. **10**, 045010 (2008)
6. Wang, L., Rastelli, A., Kiravittaya, S., Benyoucef, M., Schmidt, O.G.: Adv. Mater. **21**, 2601 (2009)
7. Schedelbeck, G., Wegscheider, W., Bichler, M., Abstreiter, G.: Science **278**, 1792 (1997)
8. Bayer, M., Hawrylak, P., Hinzer, K., Fafard, S., Korkusinski, M., Wasilewski, Z.R., Stern, O., Forchel, A.: Science **291**, 451 (2001)
9. Loss, D., DiVincenzo, D.P.: Phys. Rev. A **57**, 120 (1998)
10. Songmuang, R., Kiravittaya, S., Schmidt, O.G.: Appl. Phys. Lett. **82**, 2892 (2003)
11. Lee, J.H., Wang, Z.M., Strom, N.W., Mazur, Y.I., Salamo, G.J.: Appl. Phys. Lett. **89**, 202101 (2006)
12. Strom, N.W., Wang, Z.M., Lee, J.H., AbuWaar, Z.Y., Mazur, Y.I., Salamo, G.J.: Nanoscale Res. Lett. **2**, 112 (2007)
13. Suraprapapich, S., Thainoi, S., Kanjanachuchai, S., Panyakeow, S.: J. Vac. Sci. Technol. B **23**, 1217 (2005) [Ibid. **24**, 1665 (2006)]

14. Siripitakchai, N., Suraprapapich, S., Thainoi, S., Kanjanachuchai, S., Panyakeow, S.: J. Cryst. Growth **301**, 812 (2007)
15. Suraprapapich, S., Kanjanachuchai, S., Thainoi, S., Panyakeow, S.: Microelectron. Eng. **83**, 1526 (2006)
16. Lippen, T.v., Nötzel, R., Hamhuis, G., Wolter, J.: Appl. Phys. Lett. **85**, 118 (2004)
17. Lippen, T.v., Silov, A.Y., Notzel, R.: Phys. Rev. B **75**, 115414 (2007)
18. Thet, C.C., Sanorpim, S., Panyakeow, S., Kanjanachuchai, S.: Semicond. Sci. Technol. **23**, 055007 (2008)
19. Welsch, H., Kipp, T., Köppen, T., Heyn, C., Hansen, W.: Semicond. Sci. Technol. **23**, 045016 (2008)
20. Himwas, C., Panyakeow, S., Kanjanachuchai, S.: Nanoscale Res. Lett. **6**, 496 (2011)
21. Seravalli, L., Frigeri, P., Nasi, L., Trevisi, G., Bocchi, C.: J. Appl. Phys. **108**, 064324 (2010)
22. Nabetani, Y., Ishikawa, T., Noda, S., Sasaki, A.: J. Appl. Phys. **76**, 347 (1994)
23. Patanasemakul, N., Panyakeow, S., Kanjanachuchai, S.: Nanoscale Res. Lett. **7**, 207 (2012)
24. Krenner, H.J., Sabathil, M., Clark, E.C., Kress, A., Schuh, D., Bichler, M., Abstreiter, G., Finley, J.J.: Phys. Rev. Lett. **94**, 057402 (2005)
25. Scheibner, M., Yakes, M., Bracker, A.S., Ponomarev, I.V., Doty, M.F., Hellberg, C.S., Whitman, L.J., Reinecke, T.L., Gammon, D.: Nat. Phys. **4**, 291 (2008)
26. Beirne, G.J., Hermannstädter, C., Wang, L., Rastelli, A., Schmidt, O.G., Michler, P.: Phys. Rev. Lett. **96**, 137401 (2006)
27. Kanjanachuchai, S., Thudsalingkarnsakul, N., Siripitakchai, N., Changmoang, P., Thainoi, S., Panyakeow, S.: Microelectron. Eng. **87**, 1352 (2010)
28. Grundmann, M., Ledentsov, N.N., Stier, O., Bimberg, D., Ustinov, V.M., Kop'ev, P.S., Alferov, Z.I.: Appl. Phys. Lett. **68**, 979 (1996)
29. Mukai, K., Ohtsuka, N., Shoji, H., Sugawara, M.: Appl. Phys. Lett. **68**, 3013 (1996)
30. Lambkin, J.D., Dunstan, D.J., Homewood, K.P., Howard, L.K., Emeny, M.T.: Appl. Phys. Lett. **57**, 1986 (1990)
31. Heitz, R., Mukhametzhanov, I., Madhukar, A., Hoffmann, A., Bimberg, D.: J. Electron. Mater. **28**, 520 (1999)
32. Fafard, S., Raymond, S., Wang, G., Leon, R., Leonard, D., Charbonneau, S., Merz, J.L., Petroff, P.M., Bowers, J.E.: Surf. Sci. **361–362**, 778 (1996)
33. Szafran, B., Peeters, F.M.: Phys. Rev. B **76**, 195442 (2007)
34. Peng, J., Hermannstädter, C., Witzany, M., Heldmaier, M., Wang, L., Kiravittaya, S., Rastelli, A., Schmidt, O.G., Michler, P., Bester, G.: Phys. Rev. B **81**, 205315 (2010)
35. Thongkamkoon, N., Patanasemakul, N., Siripitakchai, N., Thainoi, S., Panyakeow, S., Kanjanachuchai, S.: J. Cryst. Growth **323**, 206 (2011)
36. Varshni, Y.P.: Physica **34**, 149 (1967)
37. Yeo, I., Dong Song, J., Lee, J.: Appl. Phys. Lett. **99**, 151909 (2011)
38. Brusaferri, L., et al.: Appl. Phys. Lett. **69**, 3354 (1996)
39. Lubyshev, D.I., Gonzalez-Borrero Jr., P.P., Marega, E., Petitprez Jr., E., La Scala, N., Basmaji, P.: Appl. Phys. Lett. **68**, 205 (1996)
40. Polimeni, A., Patane, A., Henini, M., Eaves, L., Main, P.C.: Phys. Rev. B **59**, 5064 (1999)
41. Xu, Z.Y., et al.: Phys. Rev. B **54**, 11528 (1996)
42. Yang, T., Tatebayashi, J., Tsukamoto, S., Nishioka, M., Arakawa, Y.: Appl. Phys. Lett. **84**, 2817 (2004)
43. Chia, C.K., Chua, S.J., Dong, J.R., Teo, S.L.: Appl. Phys. Lett. **90**, 061101 (2007)
44. Ngo, C.Y., Yoon, S.F., Fan, W.J., Chua, S.J.: Appl. Phys. Lett. **90**, 113103 (2007)
45. Kissel, H., Muller, U., Walther, C., Masselink, W.T., Mazur, Y.I., Tarasov, G.G., Lisitsa, M.P.: Phys. Rev. B **62**, 7213 (2000)
46. Lin, C.-F., Lee, B.-L.: Appl. Phys. Lett. **71**, 1598 (1997)
47. Haffouz, S., Raymond, S., Lu, Z.G., Barrios, P.J., Roy-Guay, D., Wu, X., Liu, J.R., Poitras, D., Wasilewski, Z.R.: J. Cryst. Growth **311**, 1803 (2009)
48. Greenwood, P.D.L., et al.: IEEE J. Sel. Topics Quantum Electron. **16**, 1015 (2010)
49. Schmitt, J.M.: IEEE J. Sel. Topics Quantum Electron. **5**, 1205 (1999)
50. Akahane, K., Yamamoto, N.: J. Cryst. Growth **323**, 154 (2011)

Temperature dependent photoluminescence and micromapping of multiple stacks InAs quantum dots

Ming Xu, Alexandre Jaffré, José Alvarez, Jean-Paul Kleider, Apichat Jittrong, Thitipong Chokamnuai, Somsak Panyakeow, Mohamed Boutchich, and Songphol Kanjanachuchai

Citation: AIP Conference Proceedings **1649**, 3 (2015); doi: 10.1063/1.4913536
View online: http://dx.doi.org/10.1063/1.4913536
View Table of Contents: http://scitation.aip.org/content/aip/proceeding/aipcp/1649?ver=pdfcov
Published by the AIP Publishing

Temperature dependent photoluminescence and micromapping of multiple stacks InAs quantum dots

Ming Xu[1, a], Alexandre Jaffré[1], José Alvarez[1], Jean-Paul Kleider[1], Apichat Jittrong[2], Thitipong Chokamnuai[2], Somsak Panyakeow[2], Mohamed Boutchich[1] and Songphol Kanjanachuchai[2]

[1]*LGEP, CNRS UMR8507, SUPELEC, Univ Paris-Sud, Sorbonne Universités - UPMC, Univ Paris 06, 11 rue Joliot-Curie, Plateau de Moulon, 91192 Gif-sur-Yvette Cedex, France*
[2]*Semiconductor Device Research Laboratory (Nanotec Center of Excellence), Department of Electrical Engineering, Faculty of Engineering, Chulalongkorn University, Bangkok 10330, Thailand*

[a)] Corresponding author: ming.xu@lgep.supelec.fr

Abstract. We utilized temperature dependent photoluminescence (PL) techniques to investigate 1, 3 and 5 stack InGaAs quantum dots (QDs) grown on cross-hatch patterns. PL mapping can well reproduce the QDs distribution as AFM and position dependency of QD growth. It is possible to observe crystallographic dependent PL. The temperature dependent spectra exhibit the QDs energy distribution which reflects the size and shape. The inter-dot carrier coupling effect is observed and translated as a red shift of 120mV on the [1-10] direction peak is observed at 30K on 1 stack with regards to 3 stacks samples, which is assigned to lateral coupling.

INTRODUCTION

Semiconductors III-V QDs are crystalline nano objects that are attractive for a wide range of detection related applications particularly in QD laser[1], near infrared region (NIR)[2] and high efficiency solar cells[3]. These nanostructures are typically grown by Molecular Beam Epitaxy (MBE) using the Stranski-Krastanow (SK) growth mechanism[4] and their small size give them interesting tunability. Indeed, the low dimensionality implies that the peak emission of QDs can be adjusted by tuning the size, composition size and passivation to suit dedicated applications. On the other hand, these objects permit the study of the transport properties of single electrons as well as advanced heterojunctions for new concepts. One major challenge remains the integration of III-V QDs on silicon substrate to develop low cost silicon photonics devices. To investigate such complex nanostructures photoluminescence has proven to be an effective tool to monitor the electronic structure as well as the optical transitions.

In this study, we employed temperature dependent macro PL characterization to investigate InAs QDs on InGaAs cross hatched patterns (CHPs) grown by MBE on (001)-GaAs substrates[5]. The structure investigated is composed of multi stack QD of 1, 3 or 5 stacks of InAs QDs and 10–nm GaAs spacer. To better understand this QDs structure, it is also important to investigate not just macroscopic PL, but also the position-dependent PL or PL mapping. For that purpose we utilized a confocal micro PL system to map the sample at room temperature and observe the crystallographic dependence of the peak emission. The temperature dependant PL spectra exhibit major differences between samples due to different QD size and lateral coupling. The PL mappings reveal position dependent luminescence[6]. These characterizations contribute to improve the understanding of the structure's optical properties, and provide a basis for future improvements on QDs based optoelectronic devices.

The Irago Conference 2014
AIP Conf. Proc. 1649, 3-7 (2015); doi: 10.1063/1.4913536

SAMPLE PREPARATION

Quantum Dots Growth

The QDs are grown on (001) GaAs substrates with MBE. After 300nm of GaAs buffer layer, the $In_xGa_{1-x}As$ CHP layer of 25-nm is firstly deposited on the substrate, followed by 10nm GaAs spacer layer then the QDs. Spacer and QDs deposition is repeated to form 3 and 5 stacks. At last, a 100nm capping layer of GaAs is deposited as passivation. The deposition of 10nm GaAs spacing layer and QDs is repeated to obtain 3 stacks and 5 stacks. Further details on the growth are reported in[5]. Another set of sample have been fabricated without capping to carry out AFM measurements. The final structure is shown in Fig.1 (a).

Morphology

AFM imaging demonstrates the QDs distribution on the topmost layer. As is shown in Fig.1 (b), the QDs are aligned along [1-10] and [110] dislocation lines while some of them distribute randomly for 1 stack. The diameter of QDs for the 1 stack sample is 30nm. For 3 and 5 stacks, almost all of the QDs align themselves along dislocation lines. Their morphology depends on the growth direction, the shape of the 1 stack QDs is circular but those of the 3 stacks and 5 stacks are prolonged along [1-10] direction. In contrast, the size of 3 stacks and 5 stacks are 35nm along [110] and 60nm along [1-10]. In addition, as the [1-10] QDs began to grow prior to the [110], and to free-standing ones, their sizes are a little different, that is, [1-10]> [110]> free-standing[7], whereas the size on both directions are similar on multiple stack samples. The distance between QDs also varies with stack number. This inter-dot distance is a key parameter to favor coupling between QDs ensembles[5]. The lateral coupling rapidly decreases as the distance increases.

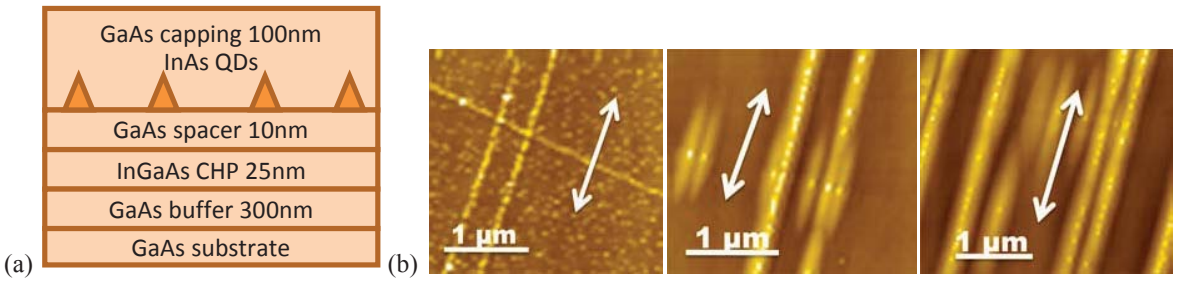

FIGURE 1. Sample structure for 1 stack sample and AFM imaging for 1, 3 and 5 stacks. Arrow in the images indicates the [1-10] direction.

TEMPERATURE DEPENDENT PHOTOLUMINESCENCE

Measurement System

Our PL system is equipped with a cryostat driven by helium circulation which allows cooling down until 20K. The excitation laser beam is projected onto the sample though cryostat window using optical fiber. The emitted luminescence is collected and focused into the monochromator and amplifier that convert photon flux to electrical signal. By controlling the monochromator, the PL spectrum is measured with a resolution of 25nm. The PL is measured under various temperatures between 30K and 300K, with a step of 10K. The sample is clamped onto the cryostat and illuminated with a 785nm laser, under a power density of 120 mW/cm^2. This power density permits only the ground state emissions. We performed several rounds of temperature measurements, from high to low as well as from low to high, to make sure that the measurement is stable and no hysteresis appears.

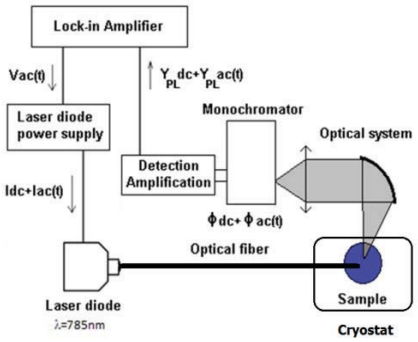

(a)

FIGURE 2. Schematic of our temperature dependent PL system

The micro PL measurements were performed with a frequency-doubled 532 nm NdYag laser operating in continuous mode as the excitation source up to 20 mW output power. The spectra were recorded through a 300 mm imaging spectrometer equipped with both 600 lines/mm and 1800 lines/mm gratings, and a back-illuminated CCD. A 100× dry and oil immersion objective with respectively a numerical aperture (NA) of 0.9 and 1.4, and a 50 µm core diameter multimode fiber acting as a pinhole were used to collect the signal. The expected lateral spatial resolution in the x-y plane can reach 150 nm (NA=1.4) and 250 nm (NA=0.9). A particular attention was paid to the incident laser power density to avoid local heating effects. A hyperspectral mapping of a 20µm by 20µm area of the sample is made possible by exciting the sample surface with 532nm laser and measuring the PL spectrum while scanning the surface using a piezoelectric stage with a spatial resolution of 10 nm.

Results

The macro PL spectra are shown in fig.2. We observe that at room temperature PL intensity is as weak as noise level, which is negligible compared to those at low temperatures. At lower temperature emission peaks begin to emerge.

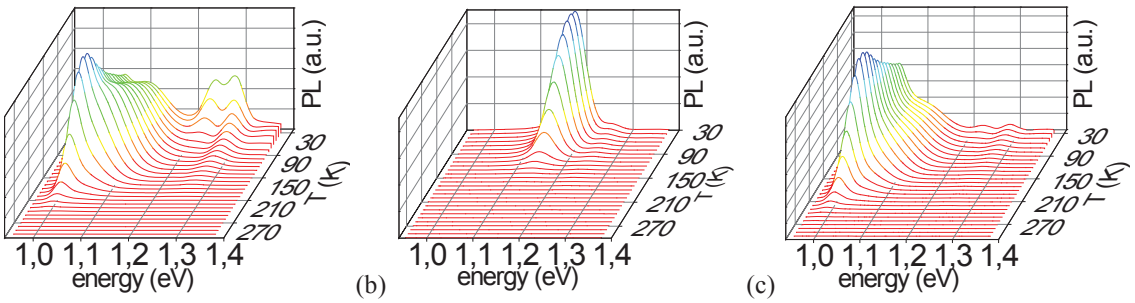

(a) (b) (c)

FIGURE 3. Temperature dependence of PL for (a) 1 stack (b) 3 stacks and (c) 5 stacks. The PL is measured every 10K from 30K to 300K.

Strong emissions minimize weaker ones when plotted in the same scale as is the case in Fig.3. We select some PL spectrums under various temperatures and rescaled them as shown in Fig.4 to give a clearer view of the emission peaks and the variation with temperature.

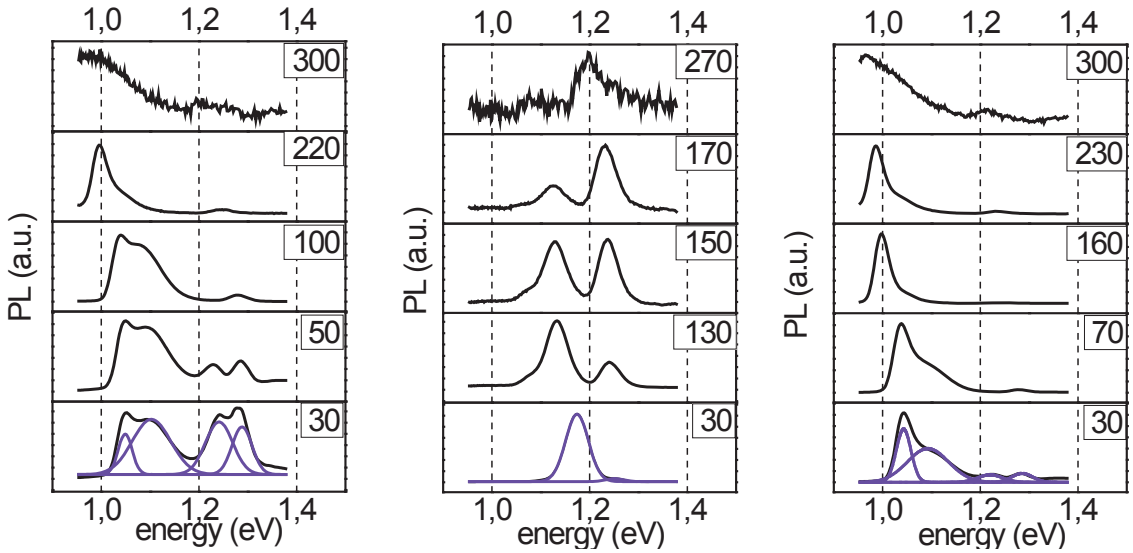

FIGURE 4. PL spectrum at some representative temperatures for 1 stack, 3 stacks and 5 stacks. Multiple Gaussian curve fitting is done for 30K to indentify peak energy. 1 stack four peaks: 1.05, 1.10, 1.24, 1.29eV; 3 stacks two peaks: 1.17, 1.25eV; 5 stacks four peaks: 1.04, 1.09, 1.22, 1.28eV

In addition to temperature dependent measurement under standard PL system, we carried out micro mapping at room temperature in order to investigate the PL distribution along the various directions. Although the PL signal is relatively low at room temperature the mapping system has enough sensitivity to resolve the PL emission from noise and the images acquired confirm the QDs distribution across specific crystallographic orientations on the surface of 1 stack sample as shown in Fig.5.

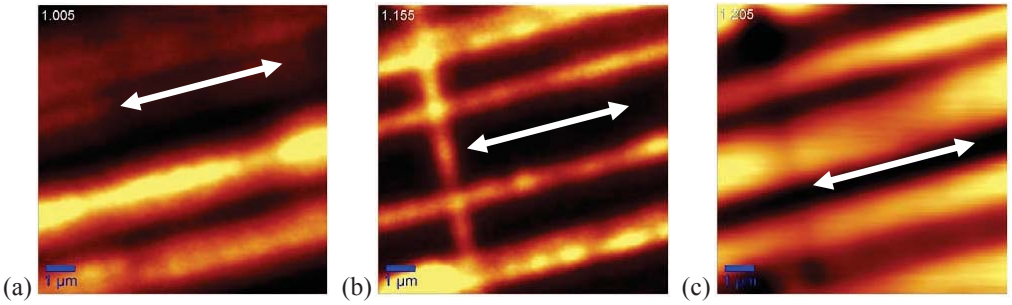

FIGURE 5. PL mapping of 1 stack at room temperature at (a) 1.005eV emission from [1-10] dots (b) 1.155eV from both [1-10] and [110] dots (c) 1.205eV from free-standing dots emission. Arrow indicates [1-10] direction.

DISCUSSION

In all samples, the emission peak of GaAs~1.42eV is not detected, indicating that the carriers generated in the GaAs and the wetting layer necessary for the growth are transferred to the QDs layer. We didn't observed vertical coupling as the spacing layer is thick enough to eliminate this effect between layers in multi-stack sample. However, strong lateral coupling is found for 1stack.

For 1 stack, we find 4 emission peaks at 30K as is shown in Fig.4 (a). In Fig.5 the first peak is located at 1.05eV, the second at 1.10eV, the third at 1.24eV and the fourth at 1.29eV. They correspond to emission of [1-10], [110] free-standing QDs and $In_xGa_{1-x}As$ CHP layer respectively[7]. Moreover, compared to 3 stacks, 1 stack has smaller QDs size but lower ground state energy in Fig4.(a)-(b). This is characterized by a red shift of 120mV on the [1-10] direction peak is observed at 30K when comparing 1 stack to 3 stacks samples. This shift is assigned to lateral coupling as discussed in [8] when the dots are very close to each other as indicated in AFM imaging.

Due to lack of free-standing QDs, the 3 stacks and 5 stacks show little of the corresponding emission. The 3-stack spectrum has two peaks and when temperature increases they both decrease as a result of thermal quenching. The intensity of the first broad peak decreases much more rapidly than the second one, making the second peak only visible at relatively higher temperature as is shown in Fig.5 (b). At 30K, the first peak is at 1.17eV and the second at 1.25eV. In fact the first peak is comprised of two closely located peaks that correspond to [1-10] and [110] dots respectively which are very close in size and shape as discussed above about Fig1.(b). The distances between QDs are bigger than 1stack, far enough not to induce coupling effect.

The behavior of 5 stacks is not similar to that of 3 stack in terms of spectra although their AFM morphology in Fig.1(b) quite resemble to each other. Inhomogeneity caused during the sample growth may be responsible for this discrepancy.

Due to the detection sensitivity, we get a noisy measurement result of 1stack at room temperature as is shown in Fig.4(a). There is a wide peak at about 1.0eV and a small one at 1.2eV. However, micro-mapping in Fig.5 demonstrates that 1.0eV emission comes from [1-10] QDs and that although we cannot see in macro-PL spectrum, [110] QDs are contributing to 1.155eV emission as shown in Fig.5(b). The 1.2eV emission should be attributed to free-standing QDs by comparing Fig.5(c) to (a) and (b).

CONCLUSION

We observed the temperature dependence of photoluminescence of multiple stack InGaAs quantum dots fabricated with MBE. The emission peaks are characteristic of the various QDs patterns present in the multi stack. In addition, using micro PL mapping, it is possible to resolve the emission peak along the crystallographic orientations and therefore identify the different QDs patterns. A blue shift of 120meV is observed on the [1-10] direction peak at 30K between the 3 and 5 stacks sample, this is assigned to the lateral coupling between dots.

ACKNOWLEDGMENTS

Authors wish to thank the French Ministère des affaires étrangères et européennes (MAEE) and the Centre National de la Recherche Scientifique (CNRS) for their financial support in the STIC ASIA program, and Thailand Research Fund (RSA5580015), as well as China Scholarship Council (CSC).

REFERENCES

[1] A. Lee, Q. Jiang, M. Tang, A. Seeds, and H. Liu, Opt. Express **20**, 22181 (2012).
[2] J.O. Kim, S. Sengupta, A.V. Barve, Y.D. Sharma, S. Adhikary, S.J. Lee, S.K. Noh, M.S. Allen, J.W. Allen, S. Chakrabarti, and S. Krishna, Appl. Phys. Lett. **102**, 011131 (2013).
[3] Y. Shoji, K. Akimoto, and Y. Okada, J. Phys. Appl. Phys. **46**, 024002 (2013).
[4] D. Leonard, M. Krishnamurthy, C.M. Reaves, S.P. Denbaars, and P.M. Petroff, Appl. Phys. Lett. **63**, 3203 (1993).
[5] T. Chokamnuai, P. Rattanadon, S. Thainoi, S. Panyakeow, and S. Kanjanachuchai, J. Cryst. Growth **378**, 524 (2013).
[6] W. Favre, J.-P. Kleider, D. Muñoz, S. Martin-de-Nicolás, and P.-J. Ribeyron, Phys. Status Solidi C **8**, 775 (2011).
[7] T. Limwongse, S. Panyakeow, and S. Kanjanachuchai, Phys. Status Solidi C **6**, 806 (2009).
[8] P. Yu, W. Langbein, K. Leosson, J.M. Hvam, N.N. Ledentsov, D. Bimberg, V.M. Ustinov, A.Y. Egorov, A.E. Zhukov, A.F. Tsatsul'nikov, and Y.G. Musikhin, Phys. Rev. B **60**, 16680 (1999).

The Effects of Long-Time Annealing of Subcritical InAs Layer on Cross-Hatch Patterns

W. Eiwwongcharoen, S. Thainoi, S. Panyakeow and S. Kanjanachuchai

Semiconductor Device Research Laboratory, Department of Electrical Engineering,
Faculty of Engineering, Chulalongkorn University, Bangkok 10330, Thailand, win.e@student.chula.ac.th

Abstract

The effects of long-time annealing of subcritical InAs layer on cross-hatch patterns are studied and characterized by atomic force microscopy and white light interferometry. Two samples were grown on (001)-GaAs by molecular beam epitaxy with 1- and 2 hours annealing time. The 2-hour-annealed sample displays more significant change in structure that 1-hour-annealed sample, as a result of increased freedom made available by additional timing. The results show a structure that is a promising candidate in broad band optoelectronic devices.

Keywords: Long-time annealing, subcritical InAs, cross-hatch patterns, molecular beam epitaxy.

1. Introduction

The miniaturization of electronic devices has been a great challenge for scientists and researchers. As the device becomes smaller, the reliability and the difficulty of reproduction are becoming more problematic. To fabricate such a small device, semiconductor nanowire can be used to help the manufacturers achieve their products with new strategies. Semiconductor nanowires have been studied for decades and have been developed to be used in many kinds of electronic devices, such as nano-transistors [1], nano-photodetectors [2], nano-sensors [3], and many other electronic devices. Nanowires have been fabricated by many methods such as metal-organic chemical vapor deposition (MOCVD) [2], metal-organic vapor phase epitaxy (MOVPE) [4] and molecular beam epitaxy (MBE) [5]. There are two ways to form nanowires, top-down or bottom-up, both have their own advantages and disadvantages. Top-down approach is easier to control the position by etching or lithography, but with low quality in nanoscale size. On the other hand, bottom-up approach has better quality in nanoscale size, but more difficult to control the position of the nanowire [6]. There is also two types of alignment in nanowire, vertical and horizontal [7]. A study shows that there are twin defect free in horizontal nanowires compare to vertical nanowires [8], which make the horizontal nanowire more ready in device fabrication [7]. In recent study, the self-assembled of horizontal Ge nanowires on Si, which is group IV, with a bottom-up approach has shown some interesting method in growing horizontal nanowires by annealing the samples by numbers of periods of time [9]. There is also many kinds of materials that can be used to fabricate nanowires, such as ZnO [10] and SiNWs (Silicon nanowires) [11]. Also in group III-V semiconductor materials, such as, InAs [1, 2, 4, 12] and GaAs [8].

In this work, we grow subcritical thickness of InAs layers on InGaAs cross-hatch patterns (CHPs) and anneal in different periods of time by molecular beam epitaxy with a bottom-up approach in mind in order to study the stability and the rearrangement of possible adatoms in the subcritical film. We used atomic force microscopy (AFM) and white light interferometry (WLI) to characterize the surface morphology. The results of this experiment shows the effects of long-time annealing.

2. Experimental Details

The cross-sectional structure of the sample under investigation is as shown in Fig. 1. Epitaxial ready (001)-GaAs substrates are used as the starting material in Riber's 32P MBE system. After oxide removal at 580°C, a 300-nm buffer layer of GaAs is grown, followed by 25-nm $In_{0.2}Ga_{0.8}As$ CHP layer, 6-nm GaAs spacer layer and 1.6 monolayer (ML) of InAs at 500°C. The growth of InAs is kept below the critical thickness, θ_c, to prevent quantum dots (QDs) from forming as a result of strain relaxation, while the pressure is kept around $8x10^{-8}$ Torr by feeding As_4 continuously. For InAs on GaAs at 500°C, θ_c is equal to 1.7 ML, we can obtain the subcritical layer with θ equal 1.6 ML by timing the change on the surface of 1.7 ML, then interpolation. Reflection high-energy electron diffraction (RHEED) is used to monitor the *in situ* pattern of the transition on the substrate's surface during growth. As soon as the InAs deposition is finished, the substrates are left for annealing with two different time periods: 1 hour and 2 hours annealing, at 490°C. After the annealing period is over, the sample is quickly cooled down to 100°C before taking out of the growth chamber. The surface of the samples is then characterized *ex situ* by atomic force microscopy (AFM) to be observed the differences between the two samples. The MSA-400 white light interferometry (WLI) is used to visualize the CHPs in 2-hour-annealed sample.

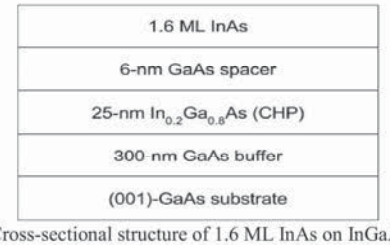

Fig. 1 Cross-sectional structure of 1.6 ML InAs on InGaAs CHPs

3. Results and Discussion

The characteristic properties of the two samples are analyzed to see the differences by using AFM scan. The lattice mismatch between InAs and GaAs is 7.2%. The InAs layer has a thickness of 1.6 ML, which is slightly below the critical thickness (1.7 ML), so QDs do not form. The 5 x 5 μm^2 AFM image and the line profile graph of the sample with 1-hour annealing is shown in Fig. 2(a-b) and those of the sample with 2-hour annealing is shown in Fig. 3(a-b), respectively.

For 1-hour annealing, the CHP is clearly shown along [1-10] direction, there are also low density InAs QDs along the line, due to the strain relaxation of the potential energy during the annealing period, as shown in Fig. 2a. We can also see the wavy lines in the image, these lines indicate that the surface is not flat, according to the line profile graph in Fig. 2b. The surface is becoming like a step, where the peak is at the CHP, which means there is higher potential energy at the CHP. The highest point has the thickness of 3 nm. The height of the QD is also shown in the inset of Fig. 2a. The QD height is 2.17 nm and the size is 9.8 nm, similar to typical InAs QD on GaAs [13].

For 2-hour annealing, the CHP has become invisible by using AFM scan, but we can see the CHP along [1-10] direction clearly with white light interferometry (WLI), as shown in Fig. 4, which we can say that the WLI scanning can see in larger area than the AFM scanning. The structure of the sample is far more than what we expected, it becomes like a hill, as shown in Fig. 3a. In Fig. 3b, we used the line profile to find the thickness of the surface, we can see that the height is in the form of steps. The thickness is around 5 nm and the length is around 3 μm, which is very interesting since the nominal thickness of InAs layer is only 1.6 ML. According to the graph, the steps have an average height around 1 nm thick. We speculate that this is due to the digging of the GaAs spacer layer or InGaAs CHP layer, since GaAs spacer layer has a thickness of 6 nm. The angles of the structure is also shown in Fig. 3a. These nano-structure is form along [110] direction, which is along the CHPs. With the different in height, the optical properties will be different from typical QDs.

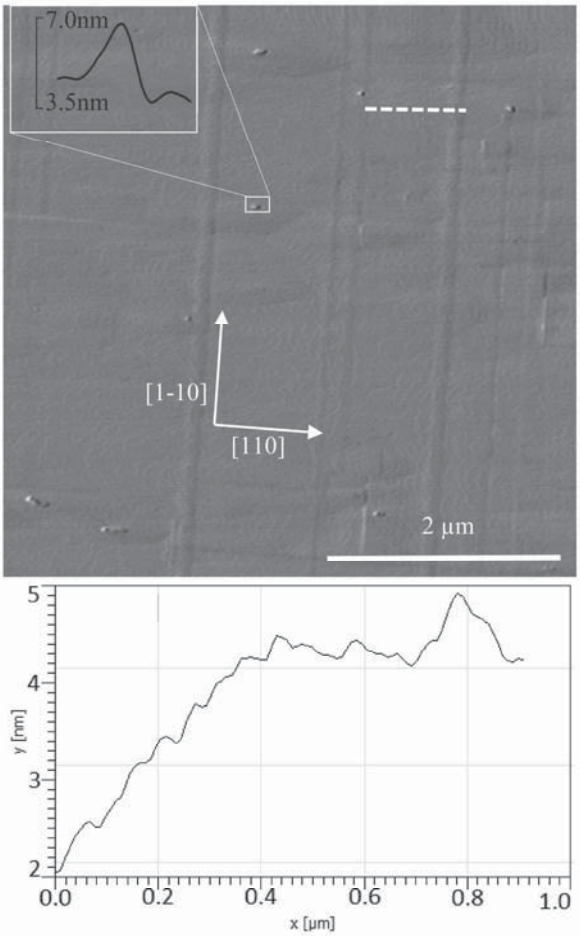

Fig. 2 (a) The 5 x 5 μm^2 AFM image of the subcritical InAs layer subject to 1-hour annealing. The inset shows the line scan across a QD. (b) Line profile along the path indicated by --- in fig(a).

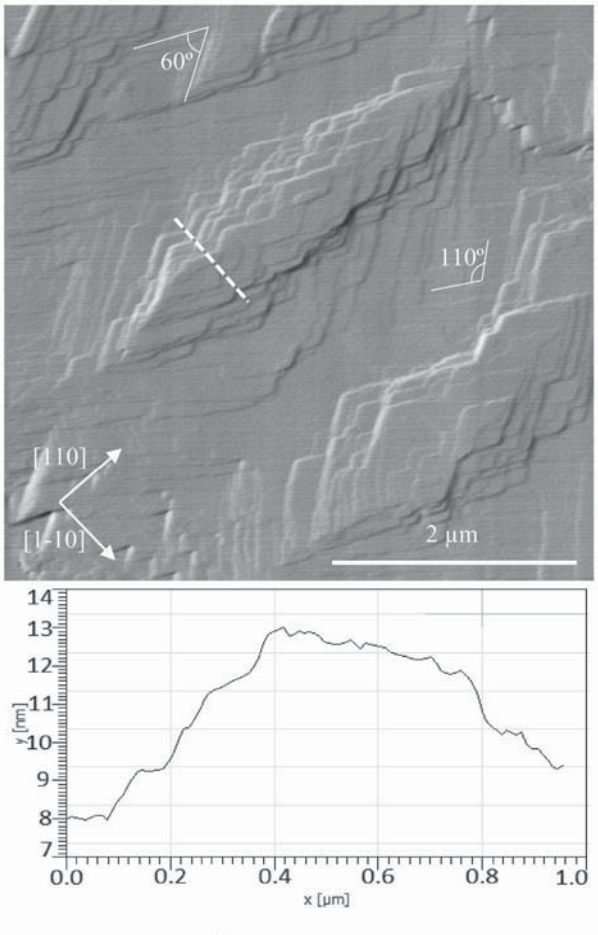

Fig. 3 (a) The 5 x 5 μm^2 AFM image of the subcritical InAs layer subject to 2-hour annealing. (b) Line profile along the path indicated by --- in fig(a).

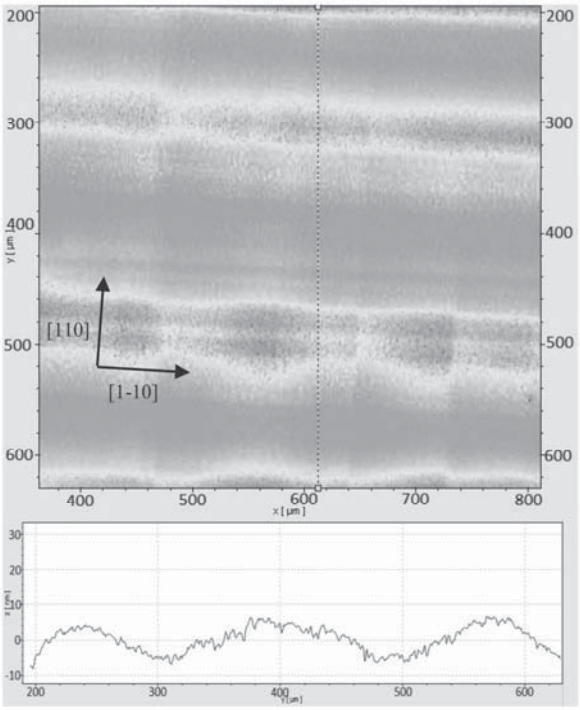

Fig. 4 WLI image of CHP and line profile of 2-hour annealing sample.

In the recent study from K. Wang and A. R. Smith, a similar structure of nanopyramids of $Mn_3N_2(001)$ grown on MgO(001) is presented [14]. The difference is in the height of the sample, where the height of Mn_3N_2/MgO is 0.6 nm with a step height of 0.202 nm, which is 10 times lower than the one in this article. The observation of the two structures could be useful in future research.

4. Conclusion

Subcritical InAs layer on cross-hatch templates is grown on epitaxial ready (001)-GaAs substrates, then annealed for 1- and 2 hours. The results show that the annealing affects the structure of the sample. For 1-hour annealing, the CHPs can still be seen, but the surrounding surface is starting to stack. For 2-hour, those stacking layer are formed into a hill-like structure. These structure could be implemented into a wider emission and absorb wavelength of light due to many heights of the structure, which will open up new applications for optical nanoelectronic devices.

Acknowledgment

This work is funded by Thailand Research Fund (RSA5580015). We thank N. Nakarcscisoon, B. A. Trisna, and A. Jittrong for help with the MBE system. We are grateful for NECTEC's Nanoelectronics & MEMS lab for access to WLI, and Dr. Anurat Wisitsora-at for assistance.

References

[1] S. Chuang et al., "Ballistic InAs Nanowire Transistors," in *Nano Letters*, 2013, 13(2), pp. 555-558

[2] Z. Liu et al., "High-detectivity InAs nanowire photodetectors with spectral response from ultraviolet to near infrared," in *Nano Research,* 2013, 6(11), pp. 775-783

[3] Y. Cui et al., "Nanowire Nanosensors for Highly Sensitive and Selective Detection of Biological and Chemical Species," in *Science,* 293, 2001, pp. 1298-1292

[4] S. Johansson et al., "Temperature and Annealing Effects on InAs Nanowire MOSFETs," in *Microelectronic Engineering,* 88(7), 2011, pp. 1105-1108

[5] F. Jabeen, S. Rubini, and F. Martelli, "Growth of III-V Semiconductor Nanowires by Molecular Beam Epitaxy," in *Microelectronics Journal,* 40, 2009, pp. 442-445

[6] H. Wang et al., "A Top-down Approach to Fabrication of High Quality Vertical Heterostructure Nanowire Arrays," in *Nano Letters,* 11, 2011, pp. 1646-1650

[7] Y. Zi, K. Jung, D. Zakharov, and C. Yang. "Understanding Self-Aligned Planar Growth of InAs Nanowires," in *Nano Letters,* 13, 2013, pp. 2786-2791

[8] S. A. Fortuna, J. Wen, I. S. Chun, and X. Li, "Planar GaAs Nanowires on GaAs(100) Substrates: Self-Aligned, Nearly Twin-Defect Free, and Transfer-Printable," in *Nano Letters,* 8(12), 2008, pp. 4421-4427

[9] J.J. Zhang et al., "Monolithic Growth of Ultrathin Ge Nanowires on Si(001)," in *Physical Review Letters,* 109, 2012, 085502(5)

[10] H. J. Fan, P. Werner, and M. Zacharias, "Semiconductor Nanowires: From Self-Organization to Patterned Growth," in *Small,* 6, 2006, pp. 700-717

[11] C. P. Lui et al., "Growth Direction and Cross-Sectional Study of Silicon Nanowires," in *Advanced Materials,* 15(8), 2003, pp. 607-609

[12] X. Zhang et al., "Evolution of Epitaxial InAs Nanowires on GaAs (111)B," in *Small,* 5(3), 2009, pp. 366-369

[13] S. Gaan, G. He, and R. M. Feenstra, "Size, shape, composition, and electronic properties of InAs/GaAs quantum dots by scanning tunneling microscopy and spectroscopy," in *Applied Physics,* 108, 2010, 114315

[14] K. Wang and A.R. Smith, "Three-Dimensional Spin Mapping of Antiferromagnetic Nanopyramids Having Spatially Alternating Surface Anisotropy at Room Temperature," in *Nano Letters,* 12, 2012, pp. 5443-5447

Polarized Photoluminescence of InAs Quantum Dots grown on InGaAs Cross-Hatch Patterns

A. Jittrong, N. Sivaarthikul, T. Chokamnuai, S. Panyakeow and S. Kanjanachuchai

Semiconductor Device Research Laboratory, Department of Electrical Engineering,
Faculty of Engineering, Chulalongkorn University, Bangkok 10330, Thailand, apichart.j@student.chula.ac.th

Abstract

This research provides the polarized photoluminescence (PPL) information of InAs quantum dots (QDs) grown on an InGaAs cross-hatch pattern (CHP) layer. The results provide the photoluminescence (PL) spectra obtained from the power and temperature dependencies to indicate the ground state energy of emissions. The PL spectra are correlated with the PPL spectra which can be used to describe the anisotropic structures by the degree of polarization (DOP). The observed DOP results are good compared with the isotopic wetting layer (WL) and bulk GaAs.

Keywords: anisotropic polarization, degree of polarization, InGaAs CHPs, InAs quantum dots

1. Background

Quantum dots (QDs) [1] are nanostructures with benefit behaviors. The structures are able to confine carriers in all 3 dimensional directions called a zero degree of freedom. The lattice mismatch in compound semiconductors can create strain in the structure. The strain relaxation activity can form the QDs where their sizes and structures define the optical properties. The quantum confinement can yield the quantized states of energy distributions so the QD structures can give the specific wavelength with a narrow bandwidth. The QDs can be applied in many applications such as QD lasers [2], photodetectors [3], and quantum information processing [4].

To control the polarization properties of optical sources is the challenging matter in many optical applications such as polarization-sensitive opto-electronic devices [5 – 6], laser diode polarization switching [7], and optical polarization modulators [8 – 9]. The conventional method to control the optical polarization is using active devices combined with passive elements such as polarizers, grating etc., resulting in the disadvantages of large sizes, less accurate alignments. Some groups have reported the studies of optical polarization controls by growth InAs/GaAs columnar QDs [10 – 12], or InP [13] QDs also QD molecules [14]. In this case the growth of InAs/AlInAs/GaAs QDs, in order to gain the high degree of polarization (DOP) about 10%, was reported in [15], 17% [16] and 32% [17].

In this paper, we propose the growth of InAs QDs on InGaAs CHPs that gives a significant DOP. The structure provides the emitted spectra of ground state emissions indicated by the power and temperature-dependent spectra. The anisotropy of QDs is observed from the DOP results according to the isotropic areas of a wetting layer (WL).

2. Sample preparation and experiment details

The schematic cross-section of the sample is shown in Fig. 1. The structure is the InAs QDs grown on the InGaAs CHP layer by Molecular Beam Epitaxy (MBE). A (001) GaAs epi-ready substrate with a 300 nm GaAs buffer layer is used to be the substrate for growing the InGaAs CHP layer. The substrate has been passed through the thermal oxide desorption at 580°C to eliminate oxides, followed by the 300 nm GaAs buffer layer with the growth rate 0.6 ML/s at 580°C. After that, the $In_{0.2}Ga_{0.8}As$ CHP layer is obtained by growing In and Ga with the growth rates 0.05 ML/s and 0.2 ML/s at 500°C under AS_4 vapor. A 25 nm thickness of the $In_{0.2}Ga_{0.8}As$ CHP layer is higher than the critical thickness required (6 nm) for strain relaxation [18]. Subsequently, a 10 nm GaAs spacer is grown over the $In_{0.2}Ga_{0.8}As$ CHP layer at 500°C of the substrate temperature. Then, the InAs QDs is grown with the critical thickness of the InAs QDs by approximately 1.7 ML [19]. The top layer of the sample is capped by a 100 nm GaAs to protect the active areas and also provide the well photoluminescence (PL) properties. Then the substrate temperature is decreased to 100°C to permanently keep the grown structure.

The experimental setup of the polarized photoluminescence (PPL) is done by using an Ar+ laser with a wavelength 514.5 nm as the exciting photons to characterize the PPL properties from the structure. A fixed linear polarizer and rotating half waveplate (HWP) are used to analyze the DOP. The sample is fixed in a chamber of cryostat systems used for temperature controls. The PPL spectra from the structure are collected by a collecting lens then focused to a monochrome. The InGaAs photodetector is used to detect the emitted spectra.

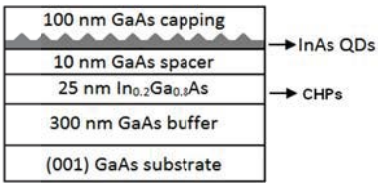

Fig. 1 Schematic cross-section of InAs QDs grown on $In_{0.2}Ga_{0.8}As$ cross-hatch pattern

3. Results and discussion

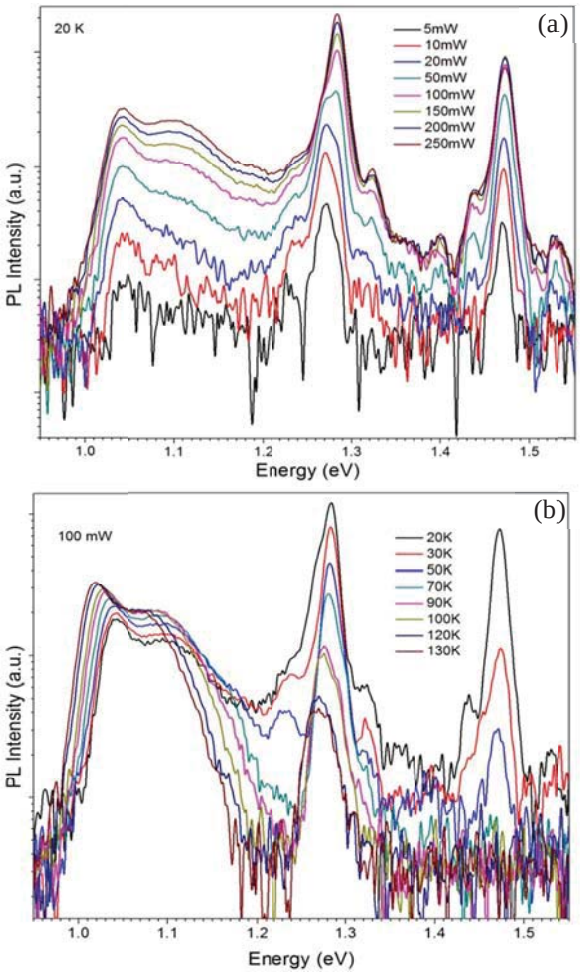

Fig. 2 PL spectra (a) power dependence (b) temparature dependence

Fig. 2 shows the PL spectra indicated by the logarithmic scales. From the power dependent spectra, the structure emits the clearly strong energy peaks of ground states at about 1.04 eV, 1.10 eV, 1.27 eV and 1.47 eV. The others are found at 1.24 eV, 1.32 eV, 1.44 eV and 1.52 eV. All peaks show the PL intensity directly increases with the increasing of the excitation powers, as shown in Fig. 2a. From the temperature dependent spectra, the energy peaks all show the redshift at the higher temperatures except for the energy peaks at 1.04 eV and 1.10 eV both show the PL intensity inverses with the increasing of the temperatures, as indicated in Fig. 2b.

To identify the peaks emitted from the structure as shown in Fig. 2a, the understanding of the nucleation sequence of InAs QDs on CHPs [20] is need. It was reported that the sequence of the QD formations is cross-hatch intersection, [1-10] misfit dislocation (MD) line, and [110] MD line, followed by the nucleation on flat areas, respectively. A dot formed early will emit the lower energy peak due to the less quantum confinement energy. So the two energy peaks at 1.04 eV and 1.10 eV should be addressed to the QDs in the [1-10] and [110] by crystallographic directions, likely reported in [21]. Consequently, the energy peak at 1.24 eV should be emitted from the QDs on the flat area or free standing dots. The strongest enegy peak at 1.27 eV is widely found as the CHP emitting [21 – 22]. Note that the CHP structure is similar to the InGaAs quantum well inserted between the GaAs buffer and GaAs spacer. For the energy peak at 1.32 eV, it is rarely found from the previous studies. However here it may potentially be emitted from the CHP due to a sufficiently anisotropic in plane polarization, as being shown in Fig. 3. The common energy peaks normally found as the WL emitting are at 1.40 eV, 1.44 eV and 1.47 eV which were also reported in [21], [23]. The final energy peak at 1.52 eV corresponds to the GaAs energy bandgap at the low temperature.

In Fig. 2b, the redshifts of energy peaks with the temperature increasing can be explained by Varshni's law [24] about reducing of energy bandgaps. The increasing of PL intensity peaks at 1.04 eV and 1.10 eV high at temperature can be explained by the carrier redistribution effects [25]. As the temperature increasing, some carriers will migrate from the WL then are trapped by the QDs having the lower energy states. So the PL intensity from the QDs becomes stronger, oppositely the PL intensity from the WL is quickly quenched.

In Fig. 3 shows the logarithmic distinction of PPL intensity measured for detailing the polarization properties. The degree of linear polarization is defined by DOP = $(I_{max} - I_{min}) / (I_{max} + I_{min})$, when I_{max} (I_{min}) which is the maximum (minimum) intensity of emitted spectra between the orthogonal directions. The DOP curve shows the highest DOP found about 26% at the energy peak 1.04 eV, consequently about 20% at energy peak of 1.10 eV. Then the emission spectra from the CHP emitting have the DOPs about 10% and 13%, as depicted in Fig. 3. The other areas show approximately isotropic structures with the nearly zero DOPs.

To explain the DOP for each of the energy peaks, accordingly the theoretical study reported that high DOPs can be majorly given from anisotropic structures and density [26]. As the structure is grown InAs QDs on the $In_{0.2}Ga_{0.8}As$ CHP layer with the sufficient critical thickness [18] then the asymmetric structures and density can be created due to the asymmetric misfit dislocations creating along the [110] and [1-10] directions. So the anisotropic structures and density of InAs QDs will be conducted by the CHPs, resulting in the high DOP at 1.04 eV and 1.10 eV. Another source of the anisotropic intensity can be piezoelectric effects that caused from shear strain and more affecting in large size QDs [27]. The different DOP result at 1.04 eV, and 1.10 eV about 6% is supposed to be caused from the piezoelectric effects that concern with the nucleation sequence.

For 10% and 13% DOPs approximately of the CHP or quantum well structure, they should be caused from t-

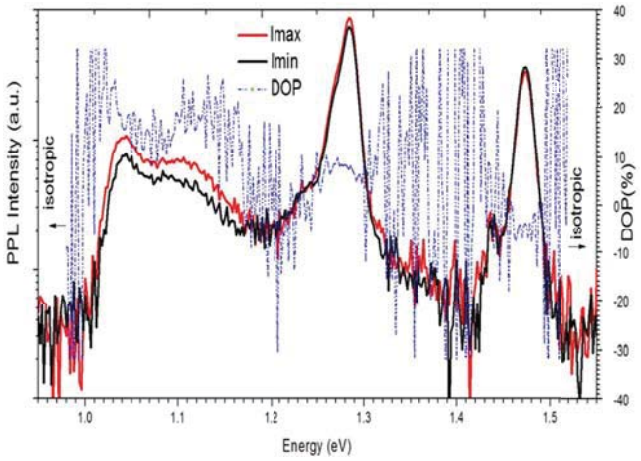

Fig. 3 PPL intensity measured for I_{max} (red), I_{min} (black) and DOP (blue) excited by 100 mW of laser power, at 20 K

he asymmetric strain relaxation or dislocation lines. In more detail, the 25 nm of thickness and the mole fraction of the $In_{0.2}Ga_{0.8}As$ should affect the DOPs of the CHP layer as Mathews and Blakeslee's critical thickness [18].

The minor DOPs of the WL and bulk GaAs together with the free standing dots can be explained by the theoretical study in [26]. As the WL and bulk GaAs structures are approximately isotropic, called as low aspect ratios, both yield the symmetry of wavefunctions leading to the low DOP results. The free standing dots as the dots form on the flat areas freely extend their isotropic sizes and which provide the minor DOP.

4. Conclusion

In conclusion, as we have shown the PL and PPL results with the DOP information. The sufficiently high DOP can be given from InAs QDs layer, and next from the InGaAs CHP layer. For the free standing dots, WL and bulk GaAs all show the isotropic wavefunctions with the small DOPs. In order to control DOP in applications more than here, the molar fraction and thickness of $GaAs/In_xGa_{1-x}$ should be included to considering together with the number of stacks.

5. Acknowledgement

This work is funded by Thailand Research Fund (RSA5580015).

References

[1] D. Bimberg et al., "Quantum dot heterostructures," *New York: Wiley.*, 1999.
[2] A. Wilk et al., "High-power 1.3 μm InAs/GaInAs/GaAs QD lasers grown in a multiwafer MBE production system," *J. Cryst. Growth.*, vol. 278(4), pp. 335 – 341, 2005.
[3] J. O. Kim et al., "Multi-stack InAs/InGaAs sub-monolayer quantum dots infrared photodetectors," *Appl. Phys. Lett.*, vol. 102, 011131, 2013.
[4] Y. Wu et al., "Coherent optical control of semiconductor quantum dots for quantum information processing," *Physica E:.*, vol. 25(2), pp. 242 – 248, 2004.
[5] P. Kiesel et al., "Polarization-sensitive opto-electronic devices based on spontaneous self-ordering in semiconductor alloys," *Materials Science & Engineering B:.*, vol. 88(2), pp. 307 – 311, 2002.
[6] P. Wiedemann et al., "MOVPE growth of ternary and quaternary tensile strained MQW structures for polarization insensitive devices," *Materials Science & Engineering B:.*, vol. 88(2), pp. 307 – 311, 2002.
[7] K. D. Choquette et al., "Vertical-cavity laser diode polarization switching and control," *J. Cryst. Growth.*, vol. 170, pp. 117 – 121, 1997.
[8] W. Niblack and E. Wolf, "Polarization modulation and demodulation of light," *Appl. Optics.*, vol. 3(2), pp. 277 – 279, 1964.
[9] H. Nour and E. Wolf, "Fluorescence nanoscopy by polarization modulation and polarization angle narrowing," *Nature Methods.*, vol. 11, pp. 579 – 584, 2014.
[10] T. Kita et al., "Polarization-independent photoluminescence from columnar InAs/GaAs self-assembled quantum dots," *Jpn. J. Appl. Phys.*, vol. 41, pp. L1143 – L1145, 2002.
[11] T. Kita et al., "Artificial control of optical gain polarization by stacking quantum dot layers," *Appl. Phys. Lett.*, vol. 88, pp. 211106, 2006.
[12] P. Ridha et al., "Polarization dependence study of electroluminescence and absorption from InAs/GaAs columnar quantum dots," *Appl. Phys. Lett.*, vol. 91, pp. 191123, 2007.
[13] K. Kawaguchi et al., "Controlling polarization of 1.55-μm columnar InAs quantum dots with highly tensile-strained InGaAsP barriers on InP(001)," *Jpn. J. Appl. Phys.*, vol. 45, pp. L1244 – L1246, 2006.
[14] C. Hermannsta et al., "Polarization anisotropic luminescence of tunable single lateral quantum dot molecules," *J. Appl. Phys.*, vol.111, 063526, 2012.
[15] D. Ochoaa et al., "Emission energy and polarization tuning of InAs/GaAs self-assembled quantum dots by growth interruption," *J. Cryst. Growth.*, vol. 251, pp. 192 – 195, 2003.
[16] N. Sellami et al., "The effect of the excitation and of the temperature on the photoluminescence circular polarization of AlInAs/AlGaAs quantum dots," *Appl. Surface Science.*, vol. 256, pp. 1409 – 1412, 2009.
[17] J.Beyer et al., "Strong room-temperature optical and spin polarization in InAs/GaAs quantum dot structures," *Appl. Phys. Lett.*, vol. 98, 203110, 2011.
[18] J. W. Matthews and A. E. Blakeslee, "Defect in epitaxial multilayers I. misfit dislocations," *Journal of Crystal Growth.*, vol. 27, pp. 118 – 125, 1974.
[19] J.M. Gérard et al., "Optical investigation of the self-organized growth of InAs/GaAs quantum boxes," *J. Cryst. Growth.*, vol. 150, pp. 351 – 356, 1995.

[20] S. Kanjanachuchai and T. Limwongse., "Nucleation sequence of InAs quantum dots on cross-hatch patterns," *J. Nanoscience and Nanotechnology.*, vol. 11, pp. 10787 – 10791 , 2011.
[21] C. Himwas et al., "Optical properties of as-grown and annealed InAs quantum dots on InGaAs cross-hatch patterns," *Nanoscale Research Letters.*, 6:496, 2011.
[22] C. C. Thet et al., "The effects of substrate mounds and pits on the periodicity of cross-hatch surface and subsequent formation of quantum dots," *Nano/Micro Engineered and Molecular Systems, 2007(NEMS 2007).*, pp. 1141 – 1144, 2007.
[23] S. Kiravittaya et al., "Multi-scale ordering of self-assembled InAs/GaAs(001) quantum dots," *Nanoscale Research Letters.*, vol.1, pp. 1 – 10 , 2006.
[24] Y. P. Varshni, "Temperature dependence of the energy gap in semiconductors", *Physica*, vol. 34, pp. 149 – 154, 1967.
[25] Y. C. Zhang et al., "Temperature dependence of electron redistribution in modulation-doped InAs/GaAs quantum dots", *J. of Cryst. Growth*, vol. 219, pp. 199 – 204, 2000.
[26] S. Weidong., "Origins of optical anisotropy in artificial atoms," *Appl. Phys. Lett.*, vol. 89, 173129, 2006.
[27] B. Gabriel and Z. Alex., "Cylindrically shaped zinc-blende semiconductor quantum dots do not have cylindrical symmetry: Atomistic symmetry, atomic relaxation, and piezoelectric effects," *Phys. Rev. B.*, vol. 71, 045318, 2013.

Self-Assembled InAs Quantum Dots Approaching Rectangular Shapes with Multi-Stacked Growth

A. Jittrong, W. Eiwwongcharoen, N. Nakareseisoon, B.A. Trisna, S. Panyakeow and S. Kanjanachuchai

Semiconductor Device Research Laboratory, Department of Electrical Engineering,
Faculty of Engineering, Chulalongkorn University, Bangkok 10330, Thailand, apichart.j@student.chula.ac.th

Abstract

A muti-stacked InAs quantum dots (QDs) is grown on an $In_{0.2}Ga_{0.8}As$ cross-hatch pattern with a small thickness of GaAs spacer by molecular beam expitaxy. The atomic force microscopy (AFM) images show the interesting shapes of the muti-stacked InAs QD structures which are approaching rectangular shapes. A high aspect ratio is given from QDs aligned in the [1-10] direction, the aspect ratio is approximately 1 along the [110] direction with the nearly square shapes.

Keywords: Atomic force microscopy, Cross-Hatch Pattern, InAs Quantum Dots, Molecular-Beam Epitaxy

1. Introduction

Since the nanotechnology has been developed, leading to the nanostructures of semiconductor devices such as quantum dots (QDs), quantum wells, quantum wires. Each of their structures has own attractive properties. Both theoretical and experimental works have been interested and studied [1 – 3]. The QDs have the confinement property called a zero dimensional degree of freedom. The structures are useful for optical devices such as QD light emitting diodes [4], QD laser [5], quantum information processing [6 – 7], resulting from their properties of high speed, low power consumption, low threshold current, and high output power.

Self-assembled InAs/GaAs QDs have been realized for optical communications at the emission wavelengths of 1.3 μm and 1.5 μm [8 – 9]. The optical properties of QDs are very sensitive from the changes in shape, size, also composition. Since the confinement energy strongly depends on the size and shape [10]. Recently, there are several studies in the QD shapes such as exciton states in quantum boxes [11], interaction of electrons in a square QDs [12], and optical properties of pyramidal InAs/GaAs QDs [13].

In this paper, we show the interesting structures of QDs which are approaching the rectangular shapes. These are attracting in optical polarization properties rather than isotropic structures. Due to there are the theoretical studies of optical polarization properties were reported that shape anisotropy and strain field majorly leading to the optical anisotropy [14 – 15]. The effects were explained by the valence-band electrons which favor to occupy the orbitals aligning along the long axis, which deals to the stronger optical emissions polarized along that axis [16].

2. Growth and characterized result

A sample is grown by a Riber 32P MBE machine. The processes are monitored by reflection high-energy electron diffraction (RHEED) streaky and spotty patterns. A semi-insulating (001) GaAs is used to be a substrate for growth the structure as show in Fig. 1. The substrate has been completed oxide desorption, then a 300 nm of GaAs buffer layer is grown at 580°C with the growth rate 0.6 ML/s for 30 minutes. After that a 25 nm of $In_{0.2}Ga_{0.8}As$ composition is grown as a template of dislocations at 500°C with the In growth rate 0.05 ML/s and Ga growth rate 0.2 ML/s, under As_4 flux of $8x10^{-6}$ torr for 5.49 minutes, the 25 nm thickness is also significant for the Matthew and Blakeslee's critical thickness of strain relaxation [17]. Consequently, a very thin layer of GaAs spacer is grown at 500°C with the growth rate 0.2 ML/s for 1.46 minutes to compete a 6 nm of a thickness. Subsequently, the five layers of InAs QDs are ready to grow with different layers separated by the 6 nm of the GaAs spacer. The first layer of the InAs QDs is grown at 610°C with the growth rate 0.18 ML/s also waiting for 20 seconds of the interruption time to improve a uniform size of the QDs. The critical thickness of the first InAs QDs layer on GaAs is approximately 1.7 ML [18]. The thicknesses of the subsequent layers are about 1.3 ML as the QDs early created before the first layer about 20 seconds. The substrate temperature is ramped down immediately to 100°C to keep the frozen QDs in sizes and structures. The surface morphology of the sample is measured by ex-situ atomic force microscopy (AFM) in air.

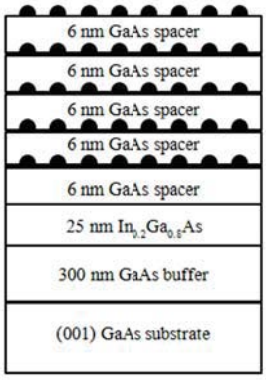

Fig. 1 Schematic cross-section of the 5 stack InAs QDs grown on $In_{0.2}Ga_{0.8}As$ cross-hatch pattern

EL009

In Fig. 2 shows the AFM images of the sample showing the surface areas and QD shapes. Fig. 2a shows the macroscopic view of the surface indicated by the 10×10 μm^2 AFM image. The formation of QDs prefers to align between the orthogonal directions, [110] and [1-10]. The morphology result demonstrates the high density of the QDs aligned in the [1-10] direction. There is a few of QDs created on the flat areas. Fig. 2b shows the microscopic view by the 2×2 μm^2 AFM image that more clearly shows the top view of the similarly rectangular shapes of the QDs. The two selected areas in the figure (white squares) are zoomed in, as shown in Fig. 2c and Fig. 2d. The QDs in the [1-10] direction that showing the shapes are asymmetric more than the [110] direction. The average aspect ratio [16] of the QDs along the [1-10] direction is about 2 which is indicating the rectangular shapes of the grown structures and reduces a-

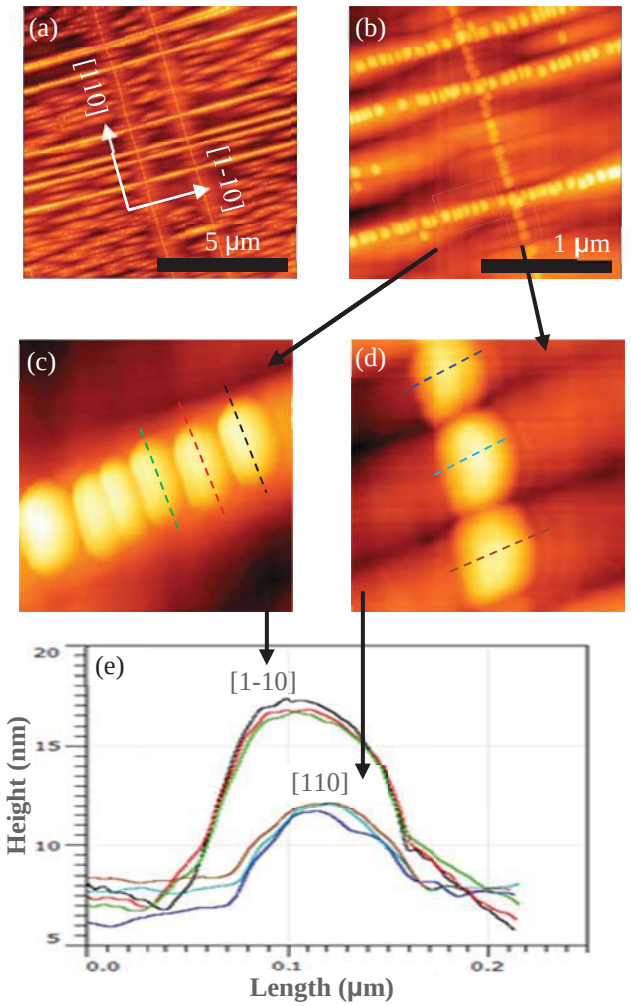

Fig. 2 (a) 10 × 10 μm^2 AFM images of InAs QDs on $In_{0.2}Ga_{0.8}As$/GaAs surfaces (b) 2 × 2 μm^2 (c) a zoom-in view of a selected area in [1-10] direction and (d) [110] direction (e) hight profile of interested dots individually measured for the dots in the [1-10] and [110] directions

pproximately to 1 for the [110] direction. The average height by a dot individually measured is depicted by the different color lines, as shown in Fig. 2e. The QDs along the [1-10] direction based on the areas is 8 nm of height and decreases to 4 nm along the [110] direction.

3. Discussion

The result of the asymmetric density of the QDs aligned along the [1-10] and [110] directions as seen in Fig. 2a can be explained by the growth of InAs QDs on GaAs/$In_xGa_{1-x}As$ substrates. As well know the growth of these elements yields misfit dislocations lying along the along <110> crystallographic directions in a (001) plan in which are termed as α and β having different structure [19] and mobility [20].These suggest the asymmetry in the dislocation density between [1-10] and [110] directions. Because of a 25 nm of $In_{0.2}Ga_{0.8}As$ thickness is significantly larger than the critical thickness (h_c) required for the misfit dislocations of about 6 nm according to Mathews and Blakeslee [17]. This will provide the asymmetric misfit dissociation lines along the orthogonal directions. Once the first InAs layer is grown then the formation will be influenced along the [1-10] rather than the [110] line and subsequently affect the top layer, and minor QDs created on the flat areas as clearly shown in Fig. 2b.

The different sizes of QDs can be explained by the sequence of QD formations. The self-assembled QDs are created by strain relaxation that will early start at the most strain areas. The sizes of QDs also depend on the nucleation sequence. The large size is formed early [20 – 21]. So in the [1-10] direction, QDs are higher and larger in size than the other direction.

There are various results in the previous studies by growth InAs QDs on InGaAs cross-hatch patterns such as without GaAs spacer, different mole fraction of $In_xGa_{1-x}As$, thickness, and a number of stacks see S. Kanjanachuchai et al. [20 – 21], same mole fraction but different thickness, and stacks see T. Limwongse et al. [22]. The closest parameter used was studied by T. Chokamnuai et al. [23]. However, those shapes of QDs were still rather circular shapes than rectangles. The approaching rectangular shape of the QDs the in [1-10] direction presented in this work should be happened from the multiple stacks of InAs QDs growth with the thin GaAs spacer. The multi-stacked structure leads to the vertical strain coupling effect between layers, it should design the shapes of the QDs on the top layer. Other things are the well lattice mismatch parameters by the chosen molar fraction of $In_xGa_{1-x}As$ with x = 0.2 together with a 25 nm of desirable growth thickness. The interesting parameter is the well thickness chosen of the GaAs spacer. The thickness is 6nm less than the previous study (10 nm) [23], it should carry the worthy parameters of strain relaxations and the required vertical coupling between layers of QDs, resulting in the rectangular shapes of the QD formations.

To explain about aspect ratios, the result shows the rectangular shapes of the QDs in the [1-10] direction that is about 2 times of the aspect ratio in the [110] direction. Even the aspect ratio is approximately 1 in the [110]

direction, but the top view of the structures looks like square more than circular shapes. The high aspect ratio in the [1-10] direction comes from the length of dots having longer in the [110] direction. This should come from the high density of the QDs created in the [1-10] line, then each dot in the line tries to extend its shape to [110] direction instead of the [1-10] direction. In the same manner, like square shapes of the QDs in the [110] direction should be caused from the lower density of the QDs created in that line then the structures are free to extend both directions, so the structures become approximately the square shapes.

4. Conclusion

As we have grown the InAs QDs on InGaAs with a thin thickness of GaAs spacer, so the shapes become rectangular in the [1-10] direction and like square shapes in the [110] direction. The result indicates that we can optimize the asymmetric structures of QD shapes by using the control of strain distribution. The number of stacks, molar fraction of $In_xGa_{1-x}As$ and thickness of GaAs spacer are good parameters to make considering for the strain distribution. These asymmetric shapes can be continued to study in the optical properties such as polarizations and emission wavelengths which are required in many applications.

5. Acknowledgement

This work is funded by Thailand Research Fund (RSA5580015).

References

[1] P. Harrison., "Quantum wells, wires and dots: theoretical and computational physics of semiconductor nanostructures," *Wiley.*, 3rd edition, 2009.

[2] M. Grundmann et al., "Nature of optical transitions in self-organized InAs/GaAs quantum dots," *Phys. Rev. B.*, vol. 53, R10509(R), 1996.

[3] D. Bimberg et al., "Quantum dot heterostructures," *New York: Wiley.*, 1999.

[4] S. Yuncheng and L.L. Minjoo., "Room temperature electroluminescence from light-emitting diodes based on $In_{0.5}Ga_{0.5}As$/GaP self-assembled quantum dots," *Appl. Phys. Lett.*, vol. 100, 251904, 2012.

[5] E. S. Semenova et al., "Metal organic vapor-phase epitaxy of InAs/InGaAsP quantum dots for laser applications at 1.5 μm," *Appl. Phys. Lett.*, vol. 99, 101106, 2011.

[6] Y. Wu et al., "Coherent optical control of semiconductor quantum dots for quantum information processing," *Physica E: Low-dimensional Systems and Nanostructures.*, vol. 25(2), pp. 242 – 248, 2004.

[7] M. V. Gurudev Dutt et al., "Semiconductor quantum dots for quantum information processing: an optical approach," *AIP Conference Proceedings.*, vol. 772, pp. 32 – 37, 2005.

[8] K. Nishi et al., "Narrow photoluminescence linewidth of 21 meV at 1.35 μm from strain-reduced InAs quantum dots covered by $In_{0.2}Ga_{0.8}As$ grown on GaAs substrates," *Appl. Phys. Lett.*, vol. 74, 1111, 1999.

[9] J. Tatebayashi et al., "Over 1.5 μm light emission from InAs quantum dots embedded in InGaAs strain-reducing layer grown by metalorganic chemical vapor deposition," *Appl. Phys. Lett.*, vol. 78, 3469, 2001.

[10] W.F. Shih and H. Jung., "Quantum-confinement effect on recombination dynamics and carrier localization in cubic InN and $In_xGa_{1-x}N$ quantum boxes," *Thin Solid Films.*, vol. 517(11), pp. 3315 – 3319, 2009.

[11] K. Yoji, and N. Katsuyuki., "Efficient numerical method for calculating exciton states," *Phys. Lett. A.*, vol. 369, pp. 128 – 131, 2007.

[12] T. Eero et al., "Two interacting electrons in a square quantum dot," *Physica E.*, vol. 40, pp. 1038 – 1041, 2008.

[13] M.K. Kuo et al., "Strain effects on optical properties of pyramidal InAs/GaAs quantum dots," *Physica E.*, vol. 26, pp. 199 – 202, 2005.

[14] S. Weidong., "Linear polarization in the emission spectra of multiexciton states in InAs/GaAs self-assembled quantum dots," *Physica E.*, vol. 40, pp. 1894 – 1895, 2008.

[15] S. Weidong., "Polarization of emission from self-assembled quantum dots and its application to the optical characterization of structure," *Phys. Status Solidi B.*, vol. 246(4), pp. 876 – 879, 2009.

[16] S. Weidong., "Origins of optical anisotropy in artificial atoms," *Appl. Phys. Lett.*, vol. 89, 173129, 2006.

[17] J. W. Matthews and A. E. Blakeslee, "Defect in epitaxial multilayers I. misfit dislocations," *Journal of Cryst. Growth.*, vol. 27, pp. 118 - 125, 1974.

[18] J.M. Gérard et al., "Optical investigation of the self-organized growth of InAs/GaAs quantum boxes," *J. Cryst. Growth.*, vol. 150, pp. 351 – 356, 1995.

[19] M.S. Abrahams et al., "Like-sign asymmetric dislocations in zinc-blende structure," *Appl. Phys. Lett.*, vol. 21, pp. 185 - 186, 1972. Creep and dislocation velocities in gallium arsenide," *Phys. status solidi (A).*, vol. 49, pp. 93-101 , 1978.

[20] S. Kanjanachuchai and T. Limwongse., "Nucleation sequence of InAs quantum dots on cross-hatch patterns," *J. Nanoscience and Nanotechnology.*, vol. 11, pp. 10787 - 10791 , 2011

[21] S. Kanjanachuchai and T. Limwongse "Complete formation sequence of InAs quantum dots on lattice-mismatched InGaAs/GaAs substrates," *Nanoelectronics Conference (INEC) 2010.*, pp. 626 - 627, 2010..

[22] T. Limwongse et al., "Evolution of InAs quantum dots grown on cross-hatch substrates," *Physica Status Solidi(c).*, vol. 6, pp. 806 - 809, 2009.

[23] T. Chokamnuai et al., “Optical properties of stacked InAs quantum dots grown on cross-hatch patterns,” *Proceeding of the 34th Electrical Engineering Conference.*, 2011.